Prepublished copy

Nature Environment & Pollution Technology

This is a peer-reviewed prepublished version of the paper to be published in Vol. 25, No. 3, September 2026 issue

Clay Brick Performance with Red Mud, Waste Foundry Sand, and Silica Fume: A Taguchi Approach

Smita S. Borchate[1], Praveen A. Ghorpade[*2], Basavaraj G. Katageri[3], Nayana P. Hoolikantimath[4],

[1] Visvesvaraya Technological University, Belagavi, Karnataka -590018, India and Department of Civil & Environmental Engineering, Kolhapur Institute of Technology's, College of Engineering (Autonomous), Kolhapur, Maharashtra-416234, India.

[*2] Department of Civil Engineering, KLE Technological University, Dr. M. S. Sheshgiri Campus, Belagavi, Karnataka-590008, India and Visvesvaraya Technological University, Belagavi-590018 India

[3] GITAM School of Technology Bengaluru Campus, Bengaluru, Karnataka, India.

[4] Department of Civil Engineering, KLE Technological University, Dr. M. S. Sheshgiri Campus, Belagavi, Karnataka - 590008, India

* Corresponding author. Email: praveenghorpade1@gmail.com

ORCID ID:

Praveen A. Ghorpade: 0000-0001-9419 -0973, Smita S. Borchate: 0000-0001-9706-2248, Basavaraj G. Katageri:0000-0002-2053-534X, Nayana P. Hoolikantimath :0000-0002-7122-2888

Key Words	Red mud, Waste foundry sand, Silica fume, Clay bricks, Geopolymerisation, Grey relational analysis
DOI	https://doi.org/10.46488/NEPT.2026.v25i03.B4390 (DOI will be active only after the final publication of the paper)
Citation for the Paper	Borchate, S.S., Ghorpade, P.A., Katageri, B.G. and Hoolikantimath, N.P., 2026. Clay brick performance with red mud, waste foundry sand, and silica fume: A Taguchi approach. *Nature Environment and Pollution Technology*, 25(3), B4390. https://doi.org/10.46488/NEPT.2026.v25i03. B4390

Abstract: The disposal of red mud (RM) and Waste Foundry Sand (WFS) poses a serious environmental concern. This study investigates the potential of utilizing these industrial by-products, along with silica fume, fly ash, and Desur clay, for the production of geopolymer clay bricks as a sustainable alternative to conventional clay bricks. Initially 5M geopolymeric clay bricks were cast by partially replacing natural clay by RM, fly ash, WFS, sodium silicate and caustic. The highest compressive strength of 3.27 N/mm^2 was obtained with 5M caustic concentration. Further, to optimize the raw material and to improve compressive strength of 5M bricks, part of the WFS was replaced with various percentages of silica fume. Grey Relational Analysis (GRA) was applied to determine the most effective mix composition, since it offers a practical platform for transforming a multi-objective function into a single-objective function. Nine mix compositions were designed using the Taguchi L9 orthogonal array. The best compressive strength of 5.02 N/mm^2 was obtained using 13.75% red mud, 10% silica fume, 12.85% WFS, 33.43% Desur clay, and 30% fly ash. The water absorption for all the sets was within permissible limits. The analysis of variance (ANOVA) shows that the silica fume (47.45%) is the most significant parameter followed red mud (30.36%). The WFS contribution was the least (21.17%) among all. Microstructural and mineralogical characterizations were conducted using Scanning Electron Microscopy

(SEM), Fourier Transform Infrared Spectroscopy (FTIR), and X-ray Diffraction (XRD), confirming the formation of geopolymeric gels and stable phases. The cast bricks were analyzed for heavy metals using Inductively Coupled Plasma (ICP), which confirmed that the developed bricks are environmentally safe for use

1. INTRODUCTION

Red mud (RM), or bauxite residue, is a by-product of Bayer's alumina-making process. Around 150 million tons of red mud is produced annually worldwide. During the manufacturing per ton of alumina, 1 to 1.5 tons of red mud is produced. The quantity of red mud depends on the quality of the bauxite ore. Initially, bauxite ore is finely ground using a ball mill in a wet process. The slurry is further digested in the digester in the presence of caustic. The alumina is dissolved in caustic, and the residue, solid mud, is termed red mud. The red mud is separated after consecutive washing. However, the residual caustic bound to the red mud is responsible high pH (11-13). Groundwater contamination from alkali seepage from red mud occurs if land disposal and lagooning methods are used. On the other hand, dry stacking produces air pollution due to its fine particle size. However, these modes need a considerable amount of land for storage and disposal; hence, they are expensive (Rai et al., 2020).

Early research showed the use of processed red mud as a material for road construction and stabilisation of acidic soil(Reddy et al., 2021) (Reddy et al., 2021). Red mud is utilised as a partial substitution for fly ash, cement, and filler material. Bricks or blocks built with stabilised red mud using 5% hydrated lime can be utilised to construct the walls of economical dwellings (Dass & Malhotra, 1990; A. Kumar et al., 2021).

The Waste Foundry Sand (WFS) is another industrial solid waste of concern generated after being worn when making moulds in metal casting industries. The foundry sand, with binders, is used frequently for casting moulds. After cyclic usage, foundry sand becomes unusable in the new moulds. Such sand is termed WFS (Matos et al., 2019). Several authors have studied its use as a natural sand, Portland cement replacement in concrete and replacement for fine aggregate to improve strength. Some authors explored using 30% WFS to replace natural sand in making clay bricks. The uses of the WFS remain a challenge, despite its application in the various uses stated above (Billong et al., 2021; Matos et al., 2019).

Silica fume (SF) is a byproduct of the silicon and ferrosilicon alloys industry. The main component of silica fume is non-crystalline silica (SiO_2), typically comprising 85 to 99% of the substance. The primary application of silica fume includes its use in parking decks, marine structures, and highway bridges as concrete and grout in oil wells, cementitious restoration products, and in refractory and ceramics (Siddique & Chahal, 2011).

Recycling industrial waste like red mud, waste foundry sand, fly ash, and silica fume promotes green construction by reducing pollution, conserving natural resources, and minimising landfill use. This approach creates eco-friendly materials, improves resource efficiency, and supports a circular economy while aligning with global sustainability goals (S. Kumar et al., 2025). Environmental regulations have become more restrictive for the safe disposal of these wastes. Due to the growing need for brick as a construction material, many researchers have attempted to utilise wastes like fly ash, sludge, wood sawdust, processed waste tea, rubber, polystyrene, waste glass, acrylic waste and limestone dust while manufacturing conventional burnt clay bricks (Ishaq et al., 2025)(Saravanan & Rao, 2023). Mineral deposits such as clay soil are exhaustively used to

manufacture conventional burnt clay bricks. Asia produces approximately 1.2 trillion clay bricks per year. About 75% of the world's clay brick is manufactured in China, India, Pakistan, and Bangladesh. India's annual utilisation of burnt clay bricks is 180 billion tons (Abbas et al., 2017). It is estimated that 350 million tons of fertile topsoil is used every year to make burnt clay bricks. To overcome the issues related to regular burnt clay bricks like greenhouse gas emission, high temperature and reduction in productivity of surrounding fertile land, the Government of India prohibits the production of clay bricks and promotes alternative building materials (Hafez et al., 2022). Bottom ash (F-class) with a highly alkaline solution can be used as a pozzolanic material. When used with a highly alkaline solution, it produces an aluminosilicate polymer due to a chemical reaction. This aluminosilicate polymer is termed a geopolymer. Apart from reducing the expense of conventional brick, the production of geopolymeric clay brick derived from fly ash facilitates the utilisation of industry-generated waste (Nandipati et al., 2023). Most research used sodium silicate and hydroxide as activators for producing geopolymeric fly ash-based bricks (Bajpai et al., 2020; Turkey et al., 2022). Considering the disposal problem inherent with red mud due to its alkalinity, various efforts have been made to neutralise it. However, the neutralisation of red mud would be uneconomical (Phoo-ngernkham et al., 2014).

Red mud has proven efficient as a geopolymer composite binding material, along with metakaolin, fly ash, coal gangue, slag, arsenic sludge, and rice husk as (Apithanyasai et al., 2020;Mudgal et al., 2021). Geopolymers constitute Si and Al tetrahedral linked with oxygen atoms in the three-dimensional structures of Calcium Silicate Hydrate (C-S-H) and Sodium aluminosilicate Hydrate (N-A-S-H) gel. The strength of this network depends on the soluble silicon dioxide and aluminium oxide from the aluminosilicate materials. Silicon dioxide from fly ash could readily disintegrate through alkali ions, but alumina from red mud dissolves more slowly. Because silica fume contains a lot of amorphous SiO_2, using it with other aluminosilicate components will increase the Si/Al ratio for the geopolymer approach. Geopolymer strength is positively impacted when the molar ratio increases because more sodium aluminosilicate hydrate gel (N-A-S-H) is created. The finer particle size of silica fume provides a large surface area and results in acceleration of the rate of reaction between the alkaline activator and aluminosilicate materials. These properties of silica fume are beneficial in increasing the geopolymer reaction (Sutar et al., 2014).

Initially, bricks were cast using WFS, fly ash with alkaline activator sodium silicate, and sodium hydroxide of two different concentrations, namely 10M and 12M. For 12 M caustic concentration bricks, the highest compressive strength of 3.5 N/mm^2 with 3.93% water absorption was achieved. These bricks showed strong efflorescence. To overcome this problem, the caustic concentration was lowered to 5M. However, these bricks' strength was 3.27 N/mm^2 (Gaonkar et al., 2023). It is important to improve the compressive strength using a 5M caustic concentration. The present work explores effectively using silica fume and red mud to increase the compressive strength.

According to the conventional procedure, multiple experiments are needed to determine the effect of different percentages of RM, SF, and WFS on the compressive strength of red mud-based geopolymeric bricks (Mohmed & Scholar, 2018; Sutar et al., 2014) (Rajesrajeswari et al., 2014). An appropriate trial design was required to minimise several experiments and evaluate the effects of individual constituents. The Taguchi

method is an effective approach for designing factors with the fewest experimentation (Rai et al., 2012). The Taguchi multi-response Grey Relational Analysis (GRA) method can also get the best set of unique factor values for several responses at once (Shivaprasad & Das, 2018).

While numerous studies have investigated the use of industrial wastes in brick manufacturing, a significant knowledge gap persists in the area of comprehensive multi-response optimization, particularly through the integrated application of Taguchi and Grey Relational Analysis (GRA) for systems involving multiple waste materials. This study addresses that gap by employing a structured Taguchi–GRA approach to optimize the combined influence of RM, SF, and WFS in clay-based brick formulations. The primary objective of the present work is to determine the optimal mix parameters that achieve a balance among mechanical strength, and water absorption under varying proportions of waste inputs. The findings highlight the effectiveness of multi-response optimization in enhancing waste valorization, offering a viable pathway for large-scale industrial reuse of hazardous and non-biodegradable wastes. This work supports sustainable construction practices by minimizing reliance on natural clay, improving environmental safety, and advancing circular economy principles within the building materials industry.

2. MATERIALS AND METHODS

2.1 Materials

The materials utilise for making bricks consisted Fly ash (Class F, JSW Energy Ltd., Ratnagiri, Maharashtra, India), Red Mud (HINDALCO Industries Ltd., Belgaum, Karnataka, India), Waste Foundry Sand (Aqua Alloys Pvt., Ltd., Shinoli, Maharashtra, India), and silica fume (Cilantro Chemicals Pvt., Ltd., Navi Mumbai, Maharashtra, India) retained 45µm < 2.0%, specific surface area Brunauer-Emmett-Teller (BET)> 19 m^2/gm, bulk density 500–700 kg/m^2), clay (Desur, Belagavi, Karnataka, India). The chemicals being used were sodium hydroxide pellets (NaOH, Nice Chemicals LR grade, 97% assay), sodium silicate (Na_2SiO_3, Sunchem Chemicals with Na_2O;16.25%, SiO_2; 34.25%, water; 49.50%), and demineralised water (conductivity < 10µS/cm).

2.2 Methodology for casting various combinations of 5M red mud Bricks using a geopolymeric approach.

Initially, screening experiments with 5M geopolymeric clay bricks were carried out by partially replacing natural clay with RM (18.79%), fly ash (30%), WFS (22.85%), sodium silicate, and caustic. The highest compressive strength of 3.27 N/mm^2 was obtained. To optimize the raw material and to improve the compressive strength of 5M bricks, part of the WFS was replaced with various percentages of silica fume, and experimental design and analysis were carried out using GAG.

2.2.1 Experimental method

The clay bricks of standard size 230 mm X 110 mm X 70 mm were cast using a hydraulic pressed brick-making machine with a pressure of 13 MPa using a geopolymeric approach. The raw materials were mixed with

geopolymeric constituents such as sodium silicate and sodium hydroxide at a ratio of 2.5 to make different sets of bricks, as shown in Table 1.

Table 1: Different material weight percentages used in various sets of geopolymer bricks in the present study.

Set of brick	RM (%)	SF (%)	WFS (%)	FA (%)	Molarity from fresh Caustic	Molarity of Caustic from Red mud
A	13.75	5	17.85	30	4.09	0.91
B	13.75	10	12.85	30	4.09	0.91
C	13.75	15	7.85	30	4.09	0.91
D	18.79	5	12.38	30	3.75	1.25
E	18.79	10	7.85	30	3.75	1.25
F	18.79	15	17.85	30	3.75	1.25
G	23.79	5	7.85	30	3.42	1.58
H	23.79	10	17.85	30	3.42	1.58
I	23.79	15	12.85	30	3.42	1.58

All raw materials, namely Desur clay, WFS, fly ash, silica fume, and red mud, were dry mixed. Followed by the addition of water and an activator. Red mud with bound caustic contained within it was used instead of some fresh caustic to prevent caustic leaching from cast bricks. The percentage of Na_2O in red mud indirectly indicates the quantity of bound caustic present.

The cast bricks were left to cure at room temperature for the entire day. To promote geopolymeric processes, those partially dry bricks were heat-cured in an oven for 24 hours at 80℃. After 24 hours, the bricks were removed from the oven and wrapped in a wet cloth for 6 days at ambient temperature. Duration of curing plays a major role in how fast and how well the geopolymer reaction occurs. Higher temperatures (like 80°C) speed up the chemical reactions that form the geopolymer bonds, while the moist curing phase helps the structure stabilize and gain strength over time. As variations in temperature and curing duration critically govern the reaction mechanisms, phase evolution, and strength development of the geopolymeric matrix. Three-dimensional silicoaluminate structures made of geopolymer are composed of connected Si and Al tetrahedral with oxygen atoms. Amorphous silica from fly ash dissolves readily in an alkaline activator, nevertheless, at room temperature, minimal alumina dissolves from red mud. Thus, in order for red mud to take part in the polycondensation process, a high temperature is required to dissolve the Al^{+4} ions from it.

The bricks were further examined for compressive strength and water absorption. The brick's compressive strength and water absorption were assessed using the standard methods described in IS-3495-1992 (Parts 1 and 2). The microstructural characterisation of these bricks was performed using XRD, SEM and Fourier Transform Infrared Spectroscopy (FTIR) techniques. The Rigaku Smart Lab diffractometer was used for the XRD study with two theta values ranging from 5° to 90° at a constant scanning speed of 1°/min using CuKα radiation (λ = 1.540 nm).

The resultant peaks were matched with the standard database, the Joint Committee on Powder Diffraction Standards (JCPDS). A Scanning Electron Microscope (MIRA3 LMH, TESCAN, Brno, Czech Republic, EU) was used to investigate the morphology of the bricks. The brick sample's FTIR spectra were recorded using a Fourier Transform Infrared spectrophotometer (BRUKER-ALPHA 100508). Each spectrum was acquired within the spectral region of 4,000–400 cm^{-1}.

Brick leachate was analysed using microwave-assisted acid digestion procedures (EPA publication SW-846 method 1311 and 3015). Accordingly, the bricks were crumbled to powder, passing through a 90 µm sieve. The sample was predigested in 5 mL of nitric acid overnight, followed by adding 10±0.1 mL of concentrated nitric acid and left to digest at 175℃ for 30 minutes. In a microwave digester, the sample was spun at 30 rpm. After the reaction, the vessel was allowed to cool. The digested sample was filtered to remove any residual particulates. Then, the samples were transferred into a volumetric flask and diluted with demineralised water to a known volume. Thus, the obtained samples were analysed for heavy metals using Inductively Coupled Plasma (ICP-MY15230013, Software Version: 7.3.0.8799, Firmware Version: 3354).

2.2.2 Multi Response optimization Grey based Taguchi method.

The Taguchi orthogonal design approach was employed for casting the red mud-based geopolymeric bricks. Three parameters, RM, SF, and WFS, were selected as variables for this study. The fly ash was kept constant at 30%. Desur clay percentage varied for red mud. The ranges and parameter levels were preferred based on earlier screening work done while preparing geopolymeric bricks (Gaonkar et al., 2023). A Taguchi array is called an orthogonal array, where at every level, one of the parameters is tested at once. The L9 orthogonal array, which contains three factors and three levels in the Taguchi method, was employed for the experiment listed in Table 2. In all, nine experiments were carried out. The compressive strength and water absorption details were triplicate samples Y1, Y2, and Y3 for compressive strength and W1, W2, and W3 for water absorption, respectively. These values were obtained per experiment of the L9 array, as shown in Table 3. For the design to work, eight Degrees of Freedom (DOF) is required.

Table 2: Factors and levels

Factors	Level 1(%)	Level 2(%)	Level 3(%)
RM	13.75	18.79	23.79
SF	5	10	15
WFS	17.85	12.85	7.85

Table 3: L9 Orthogonal array for factors and responses

Set No.	RM (%)	SF (%)	WFS (%)	Responses					
				Compressive Strength(N/mm^2)			Water Absorption (%)		
				Y1	Y2	Y3	W1	W2	W3
A	1	1	1	3.68	3.01	3.47	12.20	12.0	12.39
B	1	2	2	5.41	4.45	5.20	16.05	14.88	13.91
C	1	3	3	3.76	4.60	4.49	15.18	15.46	13.34
D	2	1	2	3.64	3.63	3.42	14.95	11.95	13.95
E	2	2	3	3.10	3.10	3.09	12.20	11.95	12.41
F	2	3	1	3.65	3.44	3.30	11.90	12.10	12.53
G	3	1	3	2.49	2.72	2.48	12.29	13.17	12.30
H	3	2	1	3.10	3.14	3.15	13.57	14.81	13.41
I	3	3	2	3.47	3.50	3.11	14.02	13.17	12.43

2.2.3 Optimisation steps for Grey based Taguchi method.

The following steps were carried out to optimise factors using Grey based Taguchi method. Additionally, these steps are demonstrated with flowchart as shown in Fig1.

Step I: Calculation of Signal-to-Noise Ratio (S/N)

To work out the S/N ratio for every response, the subsequent equation was used:

i Larger-the-better

$$\text{S/N ratio} = -10 \log_{10} \left(\frac{1}{k} \sum_{i=1}^{n} \frac{1}{x_{ij}^2} \right) \quad \ldots(1)$$

where k = number of replications and xij=observed response value, where i =1, 2, ...m; j=1, 2, ...n. This is used in experiments where maximisation of the quality characteristic is required. This is suggested to be the larger-the-better type of experiment.

ii Smaller-the-better

$$\text{S/N ratio} = -10 \log_{10} \left(\frac{1}{k} \sum_{i=1}^{n} x_{ij}^2 \right) \quad \ldots(2)$$

This is designated the smaller-the-better type experiment, where minimisation of the characteristic is required.

Step II: Normalisation of S/N ratio.

Normalisation is modifying a single data input to distribute the data uniformly and scale it into a suitable range for further analysis. The original data must be standardised using the following formula before applying the

grey relation theory to the analysis. A suitable value is subtracted from the values in the same array in order to estimate the value of this array. Use the S/N ratio value when normalising data for a grey relation analysis.

(To be used for S/N ratio, with the Larger the better manner)

$$Zij=\frac{y_{ij} - min(y_{ij}, i=1,2,\ldots\ldots n)}{max(y_{ij}, i=1,2,\ldots\ldots n)-min(y_{ij}, i=1,2,\ldots\ldots n)} \quad \ldots(3)$$

(To be used for S/N ratio, with the smaller the better manner)

$$Zij=\frac{max y_{ij}, i=1,2,\ldots\ldots n) - y_{ij}}{max(y_{ij}, i=1,2,\ldots\ldots n)-min(y_{ij}, i=1,2,\ldots\ldots n)} \quad \ldots(4)$$

*S*tep III: Calculation for absolute difference (Δ)

Δ= 1-normalize value …(5)

Step IV: Calculation of the Grey Relational Coefficient (GC)

$CG_{ij} = \frac{\Delta_{min} + \lambda \Delta_{max}}{\Delta_{ij} + \lambda \Delta_{max}}$, where λ= Distinguishing coefficient in the range 0≤ λ≤1 …(6)

The distinguishing coefficient was assigned a value between zero and one based on the responses.

Step V: Engender the Grey Relational Grade (GRG)

$$GRG = \frac{1}{m} \sum CG_{ij} \quad \ldots(7)$$

where CG_i is the Grey Relational Grade for the j^{th} response and m is the number of performance factors.

Step VI: Calculation for optimal factor and its level combination.

A factor level total table was prepared based on the GRG value for all factors and levels.

Step VII: Execute analysis of variance (ANOVA) to obtain a significant factor.

To perform ANOVA, the following steps were used:

Total variation

$$SS_T = \sum_{i=1}^{n} GRG_i^2 - CF \quad \ldots(8)$$

Were,

CF= Correction Factor

$$CF = \frac{\sum_{i=1}^{n} GRG^2}{Total\ no.of\ experiment} \quad \ldots(9)$$

a. The variation (S) for each factor and level was calculated using the same formula.

b. The Degree of Freedom (DOF) was calculated.

c. Individual degree of freedom was calculated by subtracting the number of levels from one.

d. Calculation of Error

e. The variance value (V) and the F value were calculated,

$$V = \frac{S}{DOF} \quad \ldots(10)$$

f. The percentage of the Contributing Factor (%CF).

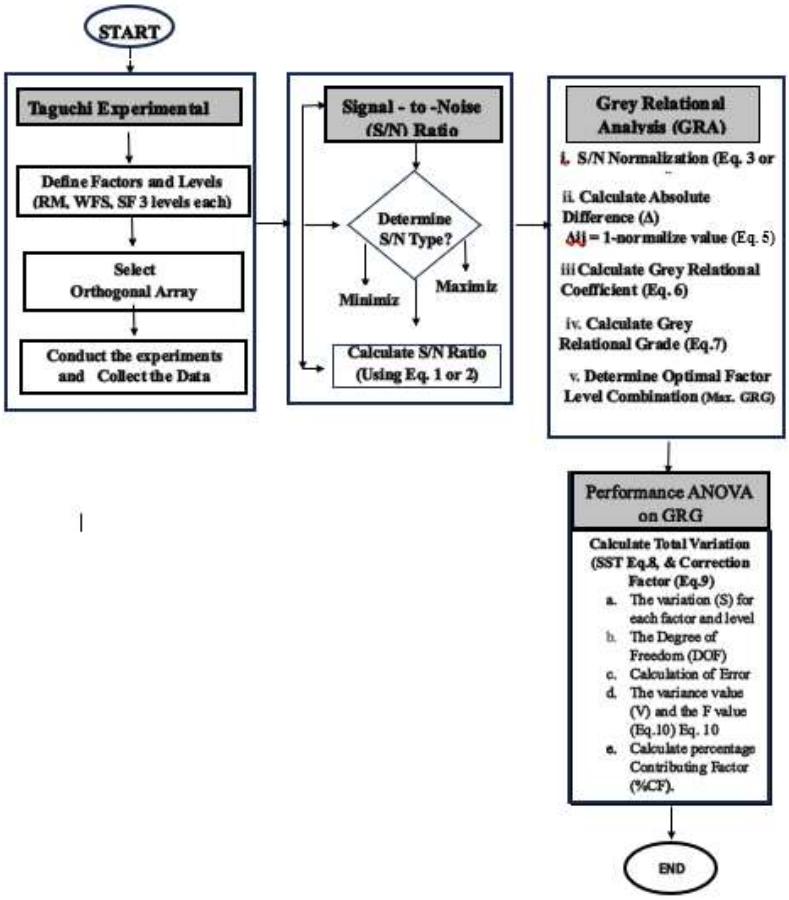

Fig. 1 Flowchart to optimise factors using Grey based Taguchi method

3. RESULTS AND DISCUSSIONS

In the present study, geopolymeric bricks were cast with red mud, silica fume, WFS, Desur clay, and constant 30% fly ash. The main constituents of red mud were Fe_2O_3 and Al_2O_3. At the same time, Desur clay had CaO, K_2O, SiO_2, and Al_2O_3 as major constituents. Silica fume contained the highest amount of SiO_2 (92%). WFS consisted of SiO_2 as a major constituent, the composition of which is represented in Table 4. The XRD plots of these materials are demonstrated in Fig. 2. The minerals in the XRD plots and the XRF oxide compositions mentioned in Table 4 are in alignment. The raw materials in the present work were selected such that their oxide compositions play a significant role in forming minerals responsible for giving strength to the clay bricks.

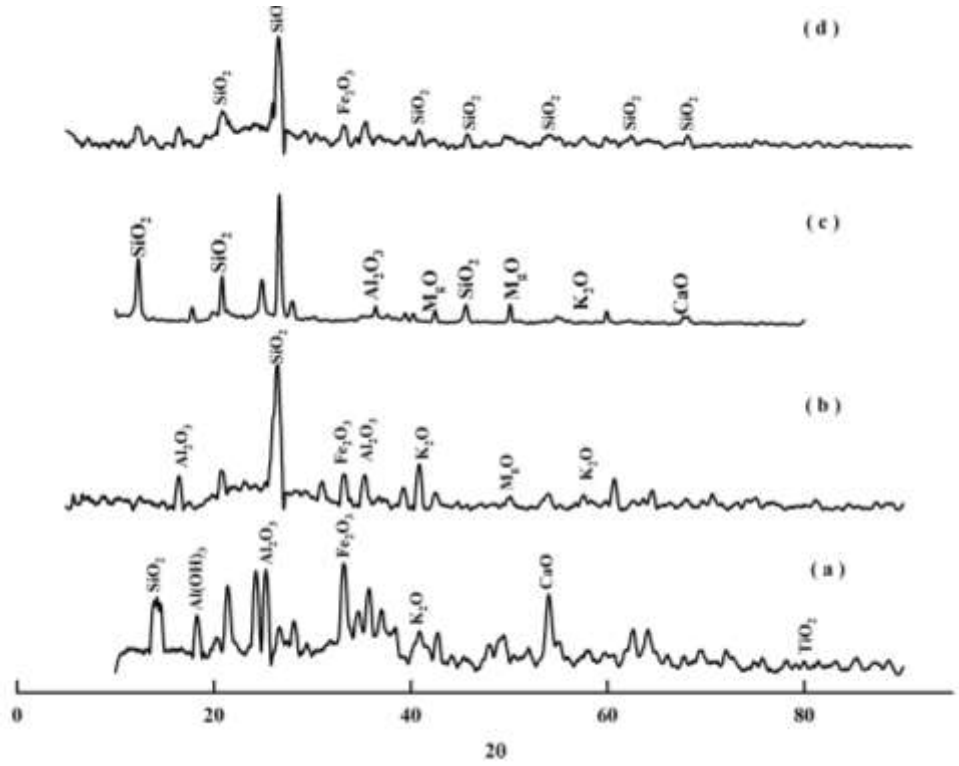

Fig. 2 XRD plot of (a) RM, (b) Fly ash, (c) Desur clay, and (d) SF.

Table 4: XRF of raw materials used in the present study.

Name of raw material	Oxide Composition % (w/w)													
	SiO_2	Al_2O_3	Fe_2O_3	Na_2O	CaO	TiO_2	P_2O_5	V_2O_5	Mn_2O_3	MgO	K_2O	MnO	Moisture	LOI
RM	10.84	20.80	39.99	5.89	3.23	6.90	0.318	0.25		-	-	-	21.40	10.6
Desur clay	57.74	28.37	8.04	0.85	0.61	1.04	0.06	-		0.64	2.44	0.03		0.08
WFS	87.91	4.70	0.94	-	0.14	0.15	-	-	0.25	0.30	0.25			5.15
SF	92.0	-	<1.0	<0.1	-	-	-	-		-	-	-	-	<3.0

Fly ash	SiO_2+ Al_2O_3+ Fe_2O_3	SiO_2	Reactive silica	SO_3	MgO	Cl	LOI
	92.3	61.34	31.11	0.01	1.01	<0.01	0.63

3.1 Compressive strength and water absorption

The subsequent segment addresses the effect of the varied weight fractions of RM, SF, and WFS on the geopolymer matrix's strength, water absorption, and microstructure in different brick sets.

3.1.1 Mineralogical Characterisation

The bricks with maximum compressive strength in each set, namely brick B from sets A, B, and C, Brick D from sets D, E, and F, and brick I from G, H, and I, were selected for studies. The raw materials in the present work were selected such that their oxide compositions play a significant role in forming sodium aluminum silicate and sodium aluminum silicate hydroxide, the geopolymeric minerals responsible for giving strength to the 5M geopolymeric clay bricks. Due to the formation of these minerals, 5 M cast bricks gain a maximum compressive strength of 5.02 N/mm² as compared to the control bricks (traditional clay bricks), which are composed of two different types of clays along with carbonaceous ash and calcined at more than 1000 °C, whose compressive strength was 3.5 N/mm².

Set B gave the highest compressive strength, and Desur clay contributes both aluminium oxide and potassium oxide, positively affecting compressive strength. Fly ash is also a source of aluminium oxide. SF is a source of reactive silica. The optimum combination of these constituents could lead to the formation of potassium sodium aluminium silicate, sodium aluminium silicate, and calcium silicate hydrate (C-S-H) as summarised in Table No. 5). The formation of potassium sodium aluminium silicate was seen at 2Ɵ values of 20.8, 26.6, 40.81, 42.4 and 59.9 (JCPDS-860683), sodium aluminium silicate at 2Ɵ value of 27.56 (JCPDS-831618), sodium aluminium silicate hydroxide at 2Ɵ values of 35.5 and 54.86 (JCPDS-832129) and C-S-H at 29.39, 30.27, 39.4 and 60.61 (JCPDS-722396). The peak of sodium aluminium silicate was attributed to the compressive strength of the brick by forming the N-A-S-H. Using red mud and activated fly ash in geopolymeric processes, researchers have proven the formation of sodium aluminium silicate and sodium aluminium silicate hydroxide geopolymeric minerals (Apithanyasai et al., 2020). These minerals are responsible for strength. The intensity for these peaks was highest in set B bricks compared to sets D and I. The area under the respective peak value of these minerals was calculated for this set of bricks. The peak area under respective peak values for these minerals is shown in Table 6.

Table 5: Minerals contributing to strength for brick sets B, D and I

2Ɵ	Name of mineral	Phase	Contribution to strength
20.8 26.6 40.81 42.42 59.9	Potassium sodium aluminium silicate	-----	Positive
27.56	Sodium aluminium silicate	N-A-S	Positive
35.50 54.86	Sodium aluminium silicate hydroxide	N-A-S-H	Positive
29.39 30.27 39.42	Calcium Silicate Hydrate	C–S–H	Positive

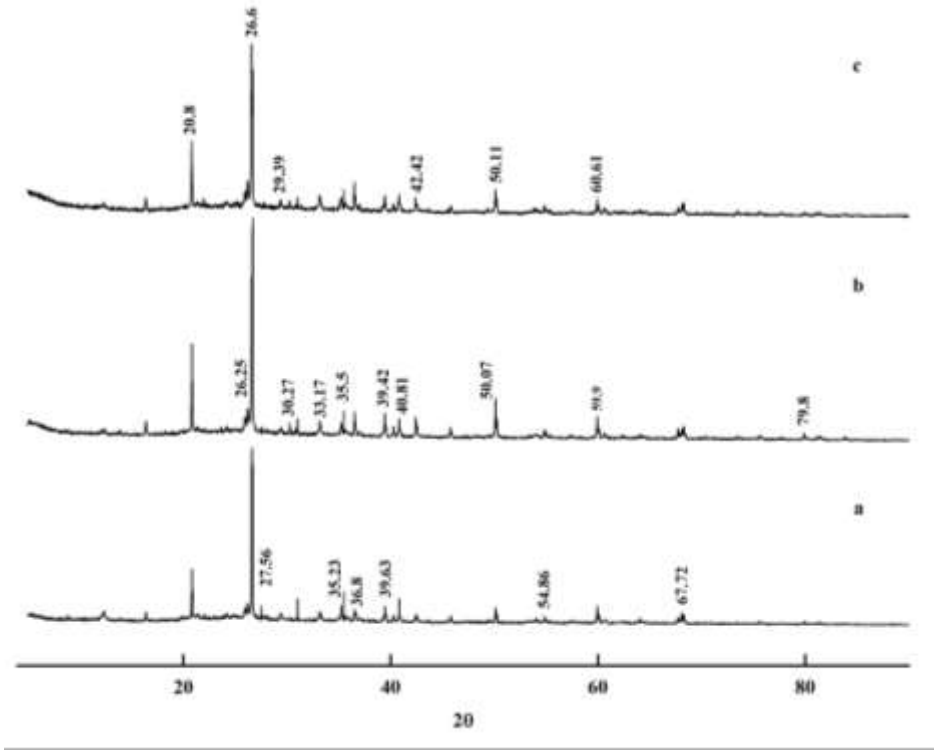

Fig. 3 XRD Analysis of (a) set B, (b) set D and (c) set I bricks.

The area under these peaks also indicated that set B had the highest peak area of these minerals compared to sets D and I. All these minerals discussed above are known to contribute towards the compressive strength of the bricks. The minor peaks of SiO_2 were seen at 2Θ values of 26.25, 39.63, 50.07 and 79.8, matching with JCPDS card no. 870703 in all the brick sets.

Table 6: Area under the peak for brick sets B, D and I.

Name of mineral	2Θ	Area under the peak for each set		
		Set B	**Set D**	**Set I**
Potassium sodium aluminium silicate	20.8	649.32	481.36	167.7
	26.6	1238.76	435.4	417.54
	40.81	224.01	173.98	101.41
	42.42	505.33	307.55	224.01
	59.9	187.0	84.82	79.98
Total area		2804.42	1483.11	990.64
Sodium aluminium silicate	27.56	87.88	25.46	23.45
Total area		87.88	25.46	23.45
Sodium aluminium silicate hydroxide	35.50	227.77	91.09	257.76
	54.86	425.36	58.50	90.25
Total area		**653.13**	**149.59**	**348.01**
Calcium Silicate Hydrate	29.39	461.1	51.16	131.41
	30.27	461.1	113.58	82.48
	39.42	134.56	131.41	114.04

	60.61	209.66	157.83	155.11
Total area		**1266.42**	**453.98**	**483.04**

The compressive strength results of different brick combinations are demonstrated in Fig. 4. Bricks set A, B, and C had 13.75% red mud, such that 0.91M of caustic from red mud contributed to the total caustic concentration of 5M. The compressive strength for sets A, B, and C was 3.38 N/mm^2, 5.02 N/mm^2, and 4.28 N/mm^2, respectively.

The second sets of bricks, D, E, and F, were cast similarly to the above, except the percentage of red mud increased from 13.75% to 18.79%, contributing to 1.25M of caustic associated with red mud. On the other hand, caustic from sodium hydroxide was reduced to 3.75M to get a total molarity of 5M. Compressive strength of 3.46 N/mm^2 for brick set F, 3.1N/mm^2 for set E and 3.56 N/mm^2 for set D were obtained.

The third set of bricks, G, H, and I, comprised 23.79% red mud, so 1.58 M of caustic from red mud contributed to the total caustic concentration of 5M. The compressive strengths for brick sets G, H, and I were 2.57 N/mm^2, 3.13 N/mm^2, and 3.36 N/mm^2, respectively.

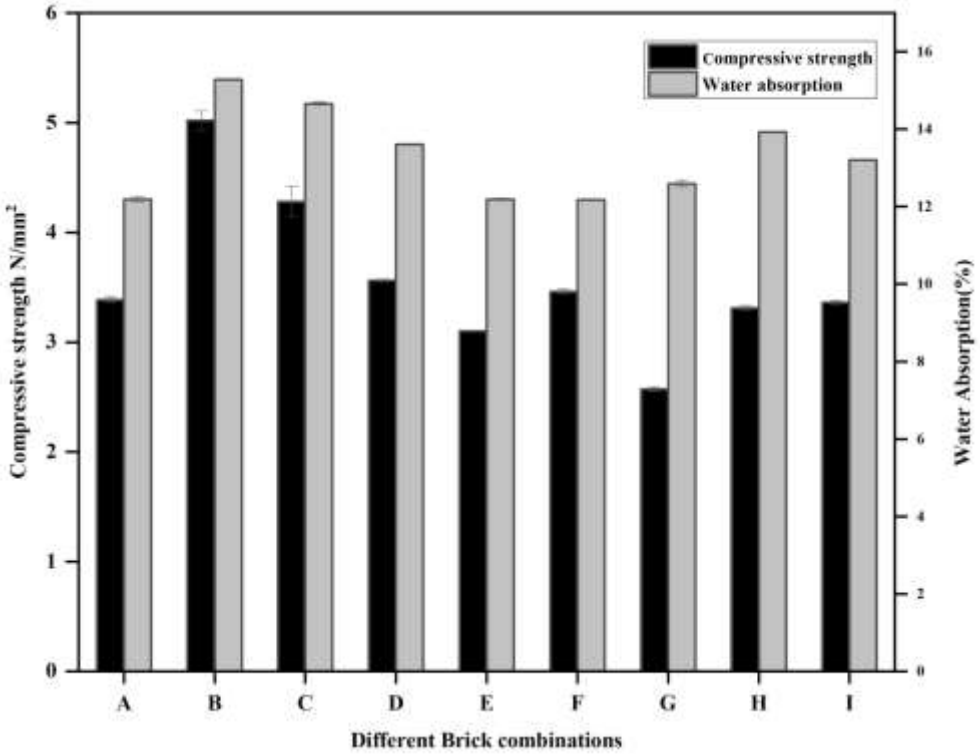

Fig. 4 Compressive strength and water absorption for different brick combinations

The first set of bricks, A, B, and C, gave maximum mean compressive strength compared to the second and third brick sets. The fresh caustic and aluminium oxide concentrations were highest in the first set. Desur clay contributes to both aluminium oxide and potassium oxide, and it induces a positive effect in gaining compressive strength. Fly ash was also a source of aluminium oxide. SF was the source of reactive silica. The optimum combination of such

constituents could lead to the formation of sodium aluminium silicate, calcium silicate hydrate, and potassium sodium aluminium silicate. The composition of these minerals is highest in the B set of bricks, which resulted in maximum compressive strength. Further, to confirm the formation of these minerals, an XRD study was performed with sets B, D, and I brick. The cast bricks B, D, and I gained the maximum compressive strength as compared to other brick combinations. The B set of bricks was cast with 10% SF, the D set of bricks was cast with 5% SF, and the I set was cast with 15% silica fume. Among these three sets of bricks maximum compressive strength of 5.02 N/mm^2 (set B) was achieved compared to 3.56 (set D) and 3.36(set I). These results clearly demonstrate that the optimal percentage of SF is important in strength reactions. If we reduce the percentage of SF from 10% to 5%, its compressive strength reduces from $5N/mm^2$ to 3.56, and if we increase it to 15 % its compressive strength reduces to 3.36 N/mm^2. Fig. 3 shows that all the brick sets passed the water absorption test, which varied between 11% and 15% and is acceptable as per IS1077:1992 standards. The dense polymeric minerals formed could fill the microscopic voids, resulting in less water absorption.

3.1.2 Scanning Electron Microscopy (SEM) Analysis

The SEM analysis is shown in Fig. 5 for brick sets B, D, and I. In set B (Fig. 4a), when 10% silica fume was used, there were fewer fly ash particles, and the matrix looked denser than in sets D and I. In addition to sodium aluminium silicate hydrate gel, calcium silicate hydrate and calcium aluminium silicate hydrate gels are also produced by fly ash and silica fume geopolymer reaction. The earlier researchers (Phoo-ngernkham et al., 2014) or calcium aluminium silicate hydrate. The inorganic polymer formed within set B (Fig. 5a) is continuous and denser than set D, leading to higher compressive strength. The unreacted silicon dioxide and aluminium oxide in fly ash and RM are embedded in the geopolymer gel phase to form a more homogeneous and dense structure. Brick sets D, and I had reduced compressive strength due to a huge quantity of unreacted fly ash and RM particles. As a result, loose and porous geopolymer gel forms, as seen in Fig. 5(b, c). Similar outcomes were reported in other literature (Shivaprasad & Das, 2018).

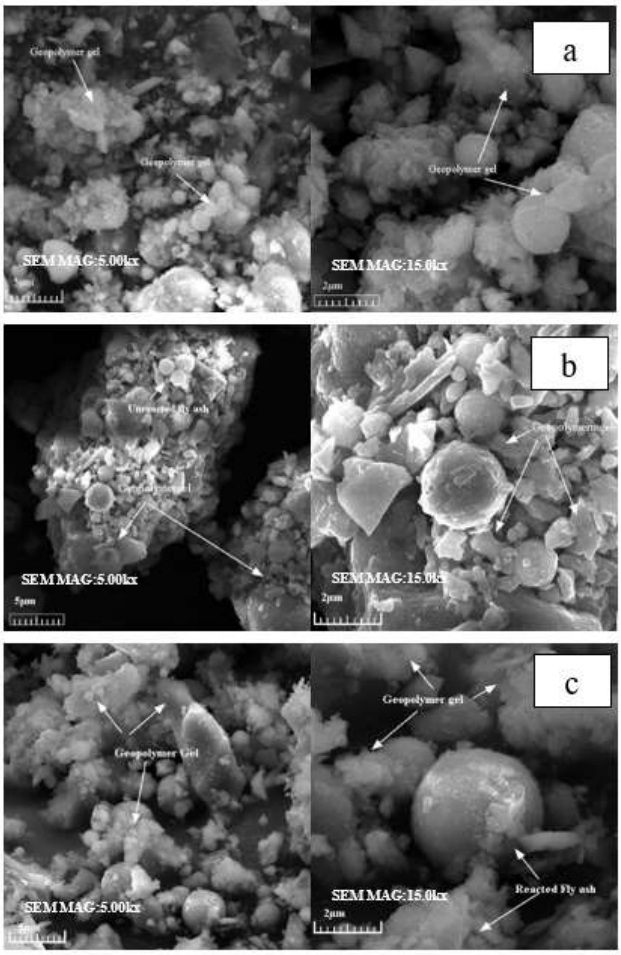

Fig. 5 SEM micrograph of (a) set B, (b) set D and (c) set I bricks. (Magnification 5000 x and 15000 x)

3.1.3 Fourier transform infrared spectrometry (FTIR) analysis.

Fig. 6 (a-c) illustrates the FTIR spectra of brick sets B, D, and I. The absorption bands at 3697 cm^{-1} and 3617 cm^{-1} are assigned to the vibration of the mode of O-H (Sontia Metekong et al., 2024). The H-OH bending vibration is represented by the bands between 1600 cm^{-1} and 1650 cm^{-1}in all three sets of bricks. Previous researchers reported similar spectra (Shill et al., 2020). The FTIR spectra at 1081.34 cm^{-1}, 1082.55 cm^{-1}, and 1082.37 cm^{-1} are allied for asymmetrical elastic oscillation regions of Si-O-Al or Si-O-Si. Similar stretching has been reported by earlier researchers (Ogundiran & Kumar, 2015). Similarly, Si-O-Si vibrations were seen at 1089.16 cm^{-1} and 1081 cm^{-1}. Spectra linked to around 465 cm^{-1} and 469.0 cm^{-1} indicate symmetric stretching and O-Si-O bending vibrations. The formation of O-Si-O (465 cm^{-1}) or Si-O-Al (1080 cm^{-1}) due to dissolution of silica from SF and alumina from RM when it comes in contact with alkaline activator at elevated temperature(80°C) during polycondensation process (Bajpai et al., 2020).The Si-O-Al bending vibration at 555 cm^{-1}, 545.5 cm^{-1}, and 790 cm^{-1} bonds of an inorganic polymer chain in all brick sets when red mud is present. The previous study reported the same finding (Jozanikohan & Abarghooei, 2022; Toniolo et al., 2017). Sodium aluminium silicate gel at peak positions 35.5 and 54.86, as shown in XRD analysis (Fig.3), is due to the

geopolymeric reaction of silicate and aluminium oxide originating from fly ash and red mud. The stretching can be correlated to the dissolution of SiO_2 and Al_2O_3.

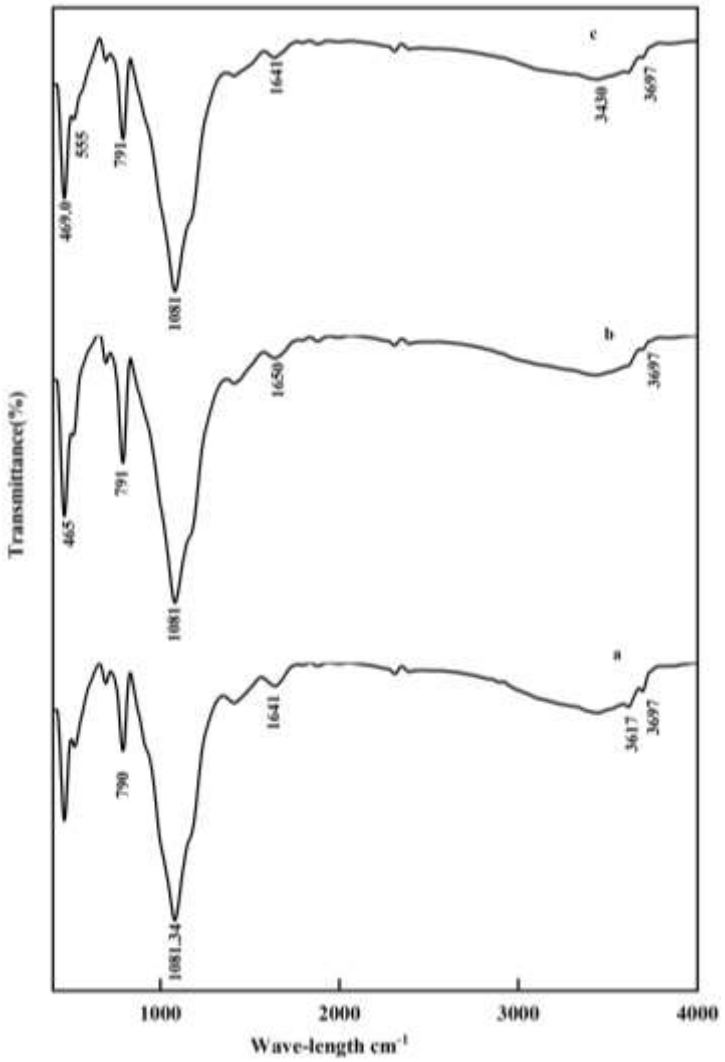

Fig.6 FTIR Analysis of (a) set B, (b) set D and (c) set I cast red mud based geopolymeric bricks.

3.1.4 Heavy metal leaching from geopolymeric bricks composed of red mud.

The geopolymeric bricks set B, D, and I were tested for leaching heavy metals. The toxicity content by the leaching protocol (EPA publication SW-846 method 1311 and 3015), was followed during the testing. The results obtained are illustrated in Table 7. Based on microwave-assisted acid digestion procedures, every element has leachabilities lower than the maximum set by the United States Environmental Protection Agency (USEPA). However, aluminium and sodium were found to leach out from these bricks. Similar results are reported in other literature. The geopolymerisation technique may not completely integrate all aluminium into the stable polymeric network, which can result in some aluminium remaining in a more reactive form. This residual reactivity may lead to the leaching of aluminium. The geopolymer framework relies on sodium ions to

counterbalance the negative charge of the aluminosilicate structure. However, some of these sodium ions are not fully integrated and can be leached out upon contact with water due to their weak binding (A. Kumar & Kumar, 2013)(Duxson et al., 2007).

Table7: The amount of the heavy metal content in the leaching solutions

	Set No.			USEPA limits (mg/L)
	B (mg/L)	D (mg/L)	I (mg/L)	
Al	129.94	75.27	78.8	-
Cd	0.00	0.00	0.00	1
Cr	0.40	0.27	0.29	5
Cu	0.14	0.10	0.10	-
Fe	112.74	71.77	75.54	-
Na	37.06	26.68	26.47	40
Ni	0.03	0.00	0.00	-
Pb	0.00	0.00	0.00	5

3.2 Analysis of data by using the Multi Response optimization Grey based Taguchi method.

The following sections discuss the effect of varied weight percentages of red mud and silica fume on compressive strength and water absorption using the multi response optimization Grey based Taguchi method in different brick sets. The statistical software package MINITAB Release 19 was used to evaluate the data from the orthogonal array experiment.

In the present work, compressive strength is a 'larger the better' form of characteristics since the aim is to optimise the strength; hence, Equation 1 of section 2.2.3 (larger-the-better) was used to assess the S/N ratio for compressive strength. Water absorption is a 'smaller-the-better' type since it has to be minimised. Equation 2 (smaller-the-better) assessed the S/N ratio for water absorption. Computed results obtained for S/N ratios, normalised S/N ratios, and absolute differences per experiment are illustrated in Table 8.

Table 8: S/N ratio, normalised S/N ratio and absolute difference

Set No.	S/N ratio		Normalised value of S/N ratios Z_{ij}		Absolute difference (Δ_{ij})	
	S/N (Compressive Strength)	S/N (Water Absorption)	Z (Compressive Strength)	Z (Water Absorption)	Δ (Compressive strength)	Δ (Water Absorption)
A	10.51	-21.72	0.42	0.00	0.58	1.00

B	13.92	-23.71	0.99	1.00	0.01	0.00
C	12.52	-23.34	0.76	0.82	0.24	0.18
D	11	-22.72	0.50	0.50	0.50	0.50
E	9.81	-21.72	0.30	1.00	0.70	0.00
F	10.60	-21.71	0.44	0.00	0.56	1.00
G	8.00	-22.01	0.00	0.15	1.00	0.85
H	9.89	-22.89	0.32	0.59	0.68	0.41
I	10.48	-22.43	0.42	0.36	0.58	0.64

The statistics of Table 8 are used to determine the grey relational coefficient using equation 6 of section 2.2.3, as demonstrated in Table 9.

The value for λ is between 0 and 1, depending on the process parameter weightage.

Table 9: Grey Relational coefficient and Grey relational grade

Set No.	**Grey Relational coefficient (GC)**		**Grey relational grade**
	GC (Compressive Strength)	GC (Water Absorption)	GRG
A	0.56	0.20	0.383
B	0.99	1.00	0.997
C	0.76	0.57	0.666
D	0.60	0.34	0.469
E	0.52	1.00	0.758
F	0.57	0.20	0.386
G	0.43	0.23	0.328
H	0.52	0.38	0.451
I	0.56	0.28	0.422

Finally, the GRG from equation 7 and the estimation model for the GRG were determined in this way,

GRG = 0.5398 + 0.1420 RM_13.75 - 0.0024 RM_18.79 - 0.1396 RM_23.79 - 0.1466 SF_5 + 0.1953 SF_10 - 0.0487 SF_15 + 0.0441 WFS_7.85 + 0.0892 WFS_12.85 - 0.1334 WFS_17.85

It is considered for optimising factors and is represented in Table 10. The ideal parameter conditions (RM1SF2WFS2) were determined by accounting for the greatest GRG in Table 11. These design conditions were in alignment with experimental Set B, as in Table 3. SF had the largest slope, followed by RM and WFS, illustrated in Fig. 7. To get maximal compressive strength, levels 1, 2, and 2 are ideal for SF, WFS, and RM,

respectively. Furthermore, this result is consistent with the requirements that match the highest GRG value in Table 11.

Table 11: Optimum Conditions

	Optimum conditions using GRG		
	RM	**SF**	**WFS**
Level 1	0.682	0.393	0.584
Level 2	0.537	0.735	0.629
Level 3	0.400	0.491	0.406
Rank	2	1	3

The main impacts of the process parameters on the mean response were also investigated using the GRG value. The average value of the quality characteristic for each factor at various levels is called the "mean response".

Table 11 displays the average GRG values for each factor at the three levels. The mean response analysis also shows the same optimal level of the parameters 1, 2, and 2 for RM, SF, and WFS, respectively (Fig. 7). Fig. 7 represents the mean GRG value of the compressive strength and water absorption of red mud-based geopolymeric bricks for the various parameters, namely RM (%), SF (%), and WFS (%). Figure 7 shows that when the RM percentage of the mixes increased from 13.75% to 23.79%, the mean GRG for compressive strength and water absorption dropped. The lower GRG value at higher RM concentration is because more Fe_2O_3 prevents fly ash from interacting and leads to less aluminosilicate gel formation. Nonetheless, as the weight percentage of SF increased from 5% to 10%, the GRG value also increased. The increase in compressive strength is related to the quantity of amorphous SiO_2 found in silica fume. When SF increases from 5% to 10%, the Si/Al ratio also increases. It causes the geopolymerisation process to form N-A-S-H gel. However, the GRG value increased with a decrease in WFS from 17.85% to 12.85% (Bajpai et al., 2020).

Table 11: Main effects on grey grades

	Levels			**For each factor-level**
Factors	**1**	**2**	**3**	**SS_T**
RM	0.682	0.537	0.400	0.119
SF	0.393	0.735	0.491	0.186
WFS	0.584	0.629	0.406	0.083

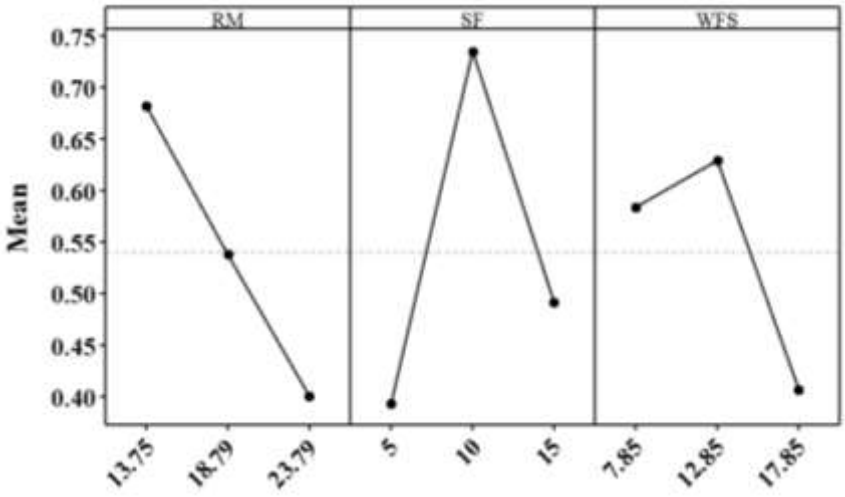

Fig.7 Main Effect Plot of GRG

Parallel lines in an interaction plot indicate no interaction between variables. In contrast, a departure from the parallel state indicates that there is no longer any interaction between the variables being studied. The mutual dependence between the variables increases with the degree of deviation from the parallel state (Montes & Allouche, 2012). From the interaction plot (Fig.8), as all lines interacted with each other, there is a significant link between the components and the GRG value because the lines in this interaction map are not parallel. Across two graphs in the first row, at 13.75% of RM, SF, and WFS greatly impacted the GRG value. However, as RM increased to 18.79%, the SF and WFS had less impact on GRG. At 23.99 % of RM, SF and WFS, they had no effect on the GRG value. The finer RM crystallised on the exterior of the coarser particles, which may have prevented the coarser particles from taking part in further reactions, which explains why SF and WFS had no effect at 23.99% of RM (Bajpai et al., 2020). In the second row of the graph, when the weight percentage of SF increased from 5% to 10%, the impact of RM and WFS increased, but it decreased to 15% of SF. The graphs in all three rows show that the maximum GRG value appears at RM level 1, SF level 2, and WFS level 2.

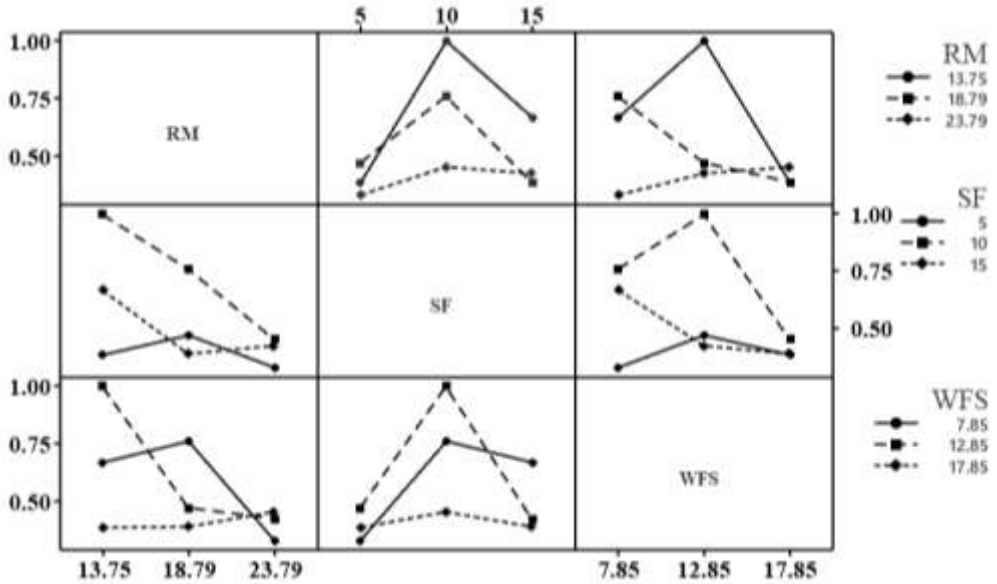

Fig.8 Interaction plot for GRG

The three-dimensional surface plot demonstrating the impact of three parameters on GRG is displayed in Fig. 9(a). Fig. 9(a) indicates that SF affected GRG more than RM. Red mud acts as filler material in the geopolymer matrix, enhancing brick compressive strength at 13.75 % of replacement. When the red mud percentage increased beyond 13.75 %, it hindered the geopolymer reaction and reduced the compressive strength of the bricks. Similar results were reported in earlier research. (Singh et al., 2020). The GRG value is larger at 12.85% of WFS and decreases as the percentage of SF increases from 10% to 15%, as shown in Fig. 9(b). SF influences GRG value as compared to the percentage of WFS. Fig. 9(c) shows that the GRG value was maximum at 10% SF and 12.85 % RM.

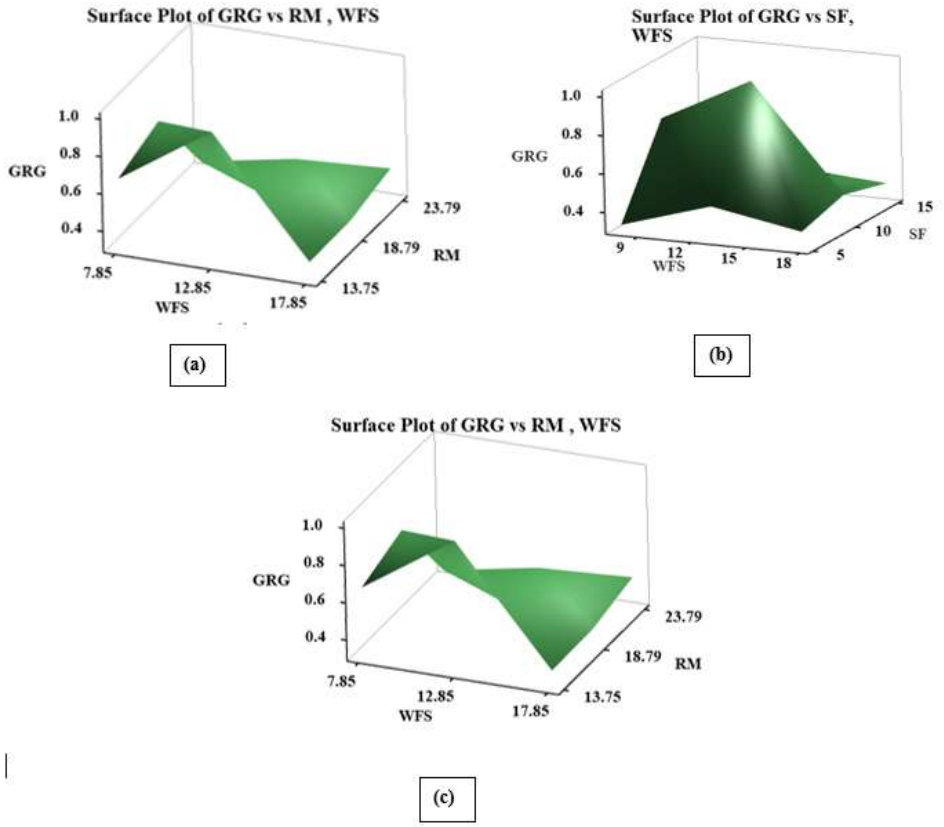

Fig.9 Surface plot: (a) The influence of SF and RM on GRG, (b) The influence of WFS and SF on GRG, (c) The influence of WFS and RM on GRG

The relative relevance of the process parameters was investigated using the ANOVA. An ANOVA was created using the GRG value to determine the important factors. Table 12 presents the outcomes of the ANOVA. RM, SF, and WFS are the significant process parameters influencing GRG, as inferred from the ANOVA table p-value of less than 0.005 at a 95% confidence level. Furthermore, each element considerably impacts compressive strength, as demonstrated by Table 12, which quantifies the F-ratio and percentage of contributions of the individual parameters in the respective columns. However, SF significantly affected the measured response, as seen by the much higher F-ratio (43.39). The ANOVA (Table 12) made it clear that the main contributors to the compressive strength and water absorption of casted geopolymeric bricks are 47.45% silica fume, followed by 30.36% red mud and 21.17%WFS. In the geopolymer process, the alkalinity plays a very

important role. In the present study, red mud-based geopolymeric bricks were cast by partial replacement of clay with varying percentages of RM, SF, and WFS with alkaline activator. Red mud used in the present study contains 5.89%(w/w) Na_2O (bound caustic). Maximum compressive strength (5N/mm^2) obtained with 10% SF and 13.75% RM due to an increase in alkalinity by RM. There is a decrease in strength as the percentage of RM and SF increases since maximum RM increases the alkalinity of the mixer, which results in fast dissolution of alumina from geopolymer procurers (RM, FA and SF) and acts as filler material and hinders the geopolymerisation process(Shivaprasad & Das, 2018) (Singh et al., 2020).

Table 12: Results of ANOVA on grey grade

Factor	SS_T	DOF	V	F	P	%CF	Conclusion
RM	0.119	2	0.059	28.14	0.034	30.36	Significant
SF	0.186	2	0.093	43.99	0.022	47.45	Significant
WFS	0.083	2	0.0415	19.64	0.048	21.17	Significant
Error	0.004	2	0.002	----	----	1.02	----
Total	0.392	8	----				

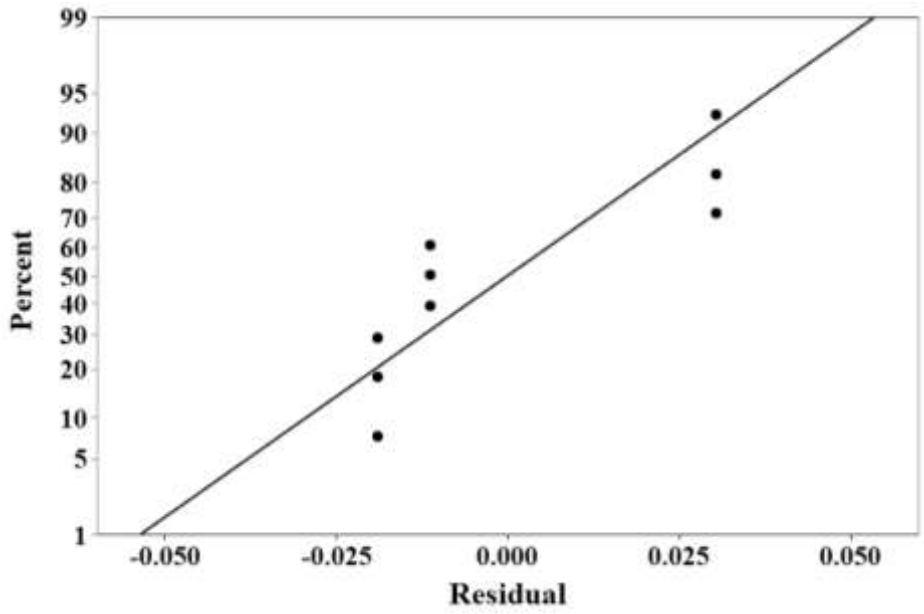

Fig.10 Normal probability plot of residual for GRG

Fig. 10 displays the normal probability plot of the GRG residual, which exhibits a straight line, indicating the effectiveness of this model.

The last phase in grey relational analysis is to predict and confirm the performance improvement of responses after the optimal factors have been determined. The predicted GRG was computed using eq. 11. To

validate the analysis's findings, confirmation tests were performed, and the average GRG over three runs was computed. Also, Table 13 demonstrates that the confirmation experiments' findings are in consistent with the predicted values.

$$\text{GRG predicted} = GRG_m + \sum_{i=1}^{q} GRG_o - GRG_m \quad \ldots (11)$$

Where GRG_o denotes the maximum of average at optimal level of factors GRG and GRG_m reparents mean GRG. Number of factors reparent by q.

Table13.Results of the confirmation experiment.

	Optimal Design Parameters	
	Prediction	Experiment
Optimal Factors Level	RM1 SF2 WFS2	RM1 SF2 WFS2
GRG	0.967	0.997

4. CONCLUSIONS.

Higher compressive strength resulted from the continuous and denser inorganic polymer generated within set B compared to set D. The unreacted silicon dioxide and aluminium oxide in fly ash and RM are embedded in the geopolymer gel phase to create a more uniform and solid structure. The aluminosilicate gel formed during geopolymerization plays a crucial role in immobilizing metallic species through mineral encapsulation, ion exchange, and physical entrapment within a highly cross-linked aluminosilicate network. The dense structure and stable Si–O–Al bonding reduce metal mobility by minimizing pore connectivity and leachable phases. The findings showed that the highest compressive strength of 5.02 N/mm^2 in set B was achieved with optimum red mud, silica fume and fresh caustic concentration. Leachability studies showed that these bricks have hazardous trace elements that are much below USEPA limits, making them environmentally safe. The cost optimisation of such bricks and long-term evaluation of geopolymeric strength remains a scope for future work. The present work focused on gaining the best compressive strength with 5M total caustic concentration in clay bricks consisting of the optimised proportion of red mud, Desur clay, silica fume and caustic. The other constituents included WFS and fly ash. The amalgamation of 13.17% (level 1) of red mud, 10% (level 2) of silica fume, and 12.85% (level 2) based on GRG were the optimised parameters. Based on the results of the ANOVA of GRG, it was found that the substitution of silica fume (47.45%) contributed the most, and red mud (30.36%) had the second-highest contribution to the response values. The WFS contribution was the least (21.17%) among all. These optimum conditions were in alignment with experimental Set B. Furthermore, the future research should involve long-term durability and leachability assessments through aging tests such as prolonged water immersion, cyclic wetting–drying, and exposure to weak acids to evaluate potential metal release under aggressive environmental conditions.

Author Contributions:

Following is the author's contribution in writing the original draft

First Author - Smita S. Borchate- Formal analysis, investigation, writing original draft.

Second Author- Praveen A. Ghorpade- Conceptualisation, methodology, validation, writing original draft, visualisation, supervision, and project administration.

Third Author- Basavaraj G. Katageri - Supervision and project administration.

Fourth Author – Nayana P Hoolikantimath - Investigation, conceptualisation and writing original draft.

Funding:

No funds, grants, or other support were received for this research work.

Acknowledgement

The authors are grateful to the Department of Civil Engineering, KLE Technological University, M. S. Sheshgiri Campus, Belagavi, for providing the necessary institutional facilities. The authors would also like to thank Kolhapur Institute of Technology's College of Engineering (Autonomous), Kolhapur, India, for permitting us to perform laboratory work. The red mud used in this work was supplied by HINDALCO Industries Ltd., Belgaum, Karnataka, India and is greatly acknowledged. The authors greatly appreciate the help of the Physics Department, Shivaji University, Kolhapur, Maharashtra, for SEM analysis. The authors also acknowledge the Common Facility Centre, Shivaji University, Kolhapur, for providing XRD and TCLP analysis facilities.

Conflicts of Interest:

The authors declare no conflicts of interest.

REFERENCES

1. Abbas, S., Saleem, M. A., Kazmi, S. M. S., and Munir, M. J. (2017). Production of sustainable clay bricks using waste fly ash: Mechanical and durability properties. *Journal of Building Engineering*, 14, pp.7–14. https://doi.org/10.1016/j.jobe.2017.09.008
2. Apithanyasai, S., Supakata, N., and Papong, S. (2020). The potential of industrial waste: using foundry sand with fly ash and electric arc furnace slag for geopolymer brick production. *Heliyon*, 6(3), pp. e03697. https://doi.org/10.1016/j.heliyon.2020.e03697
3. Bajpai, R., Shrivastava, A., and Singh, M. (2020). Properties of fly ash geopolymer modified with red mud and silica fume: a comparative study. *SN Applied Sciences*, 2(11), 1846. https://doi.org/10.1007/s42452-020-03665-3

4. Billong, N., Oti, J., and Kinuthia, J. (2021). Using silica fume based activator in sustainable geopolymer binder for building application. *Construction and Building Materials*, 275, pp. e122177. https://doi.org/10.1016/j.conbuildmat.2020.122177
5. Dass, A., and Malhotra, S. K. (1990). Lime-stabilized red mud bricks. *Materials and Structures*, 23, pp.252–255. https://doi.org/10.1007/BF02472198
6. Duxson, P., Mallicoat, S. W., Lukey, G. C., Kriven, W. M., and van Deventer, J. S. J. (2007). The effect of alkali and Si/Al ratio on the development of mechanical properties of metakaolin-based geopolymers. *Colloids and Surfaces A: Physicochemical and Engineering Aspects*, 292(1), pp.8–20. https://doi.org/10.1016/j.colsurfa.2006.05.044
7. Gaonkar, P. V., Bevinakatti, S., Hoolikantimath, N. P., Borchate, S. S., Katageri, B. G., and Ghorpade, P. A. (2023). A Geopolymeric Approach to Utilize the Bound Caustic of Bayer's Red Mud and Waste Foundry Sand in Clay Brick. *Indian Geotechnical Journal*, 53(2), pp.473–483. https://doi.org/10.1007/s40098-022-00683-3
8. Hafez, R. D. A., Tayeh, B. A., and Abd- Al Ftah, R. O. (2022). Development and evaluation of green fired clay bricks using industrial and agricultural wastes. *Case Studies in Construction Materials*, 17, pp. e01391. https://doi.org/10.1016/j.cscm.2022.e01391
9. Ishaq, M., Ali, A., Hussain, A. A., Kamran, K., Ghuffar, A., and Anwar, A. (2025). Industrial waste as clay substitute in brick manufacturing. *Construction and Building Materials*, 477. pp. 141359 https://doi.org/10.1016/j.conbuildmat.2025.
10. Jozanikohan, G., and Abarghooei, M. N. (2022). The Fourier transform infrared spectroscopy (FTIR) analysis for the clay mineralogy studies in a clastic reservoir. *Journal of Petroleum Exploration and Production Technology*, 12(8), pp.2093–2106. https://doi.org/10.1007/s13202-021-01449-y
11. Kumar, A., and Kumar, S. (2013). Development of paving blocks from synergistic use of red mud and fly ash using geopolymerization. *Construction and Building Materials*, 38, pp.865–871. https://doi.org/10.1016/j.conbuildmat.2012.09.013
12. Kumar, A., Saravanan, T. J., Bisht, K., and Kabeer, K. I. S. A. (2021). A review on the utilization of red mud for the production of geopolymer and alkali activated concrete. *Construction and Building Materials*, 302, pp.187–192. https://doi.org/10.1016/j.conbuildmat.2021.124170
13. Kumar, S., Ansari, M. A., Kant, L., and Nand, N. (2025). An Experimental Investigation on Sustainable Concrete Made with Refractory Brick as a Substitute of Natural Fine Aggregate. *Nature Environment and Pollution Technology*, 24(1). https://doi.org/10.46488/NEPT.2025.v24i01.B4202
14. Matos, P. R. de, Marcon, M. F., Schankoski, R. A., and Prudêncio, L. R. (2019). Novel applications of waste foundry sand in conventional and dry-mix concretes. *Journal of Environmental Management*, 244, pp. 294–303. https://doi.org/10.1016/j.jenvman.2019.04.048
15. Mohmed, A., and Scholar, A. B. (2018). Studies on Role of Silica Fume in Geopolymer Concrete and its Properties. *International Journal of Civil Engineering and Technology (IJCIET)*, 9(7), pp. 112–122.
16. Montes, C., and Allouche, E. (2012). Influence of Activator Solution Formulation on Fresh and Hardened Properties of Low-Calcium Fly Ash Geopolymer Concrete. *Coal Combustion and Gasification Products*, 4(1), pp. 1–9. https://doi.org/10.4177/CCGP-D-10-00017.1
17. Mudgal, M., Singh, A., Chouhan, R. K., Acharya, A., and Srivastava, A. K. (2021). Fly ash red mud geopolymer with improved mechanical strength. *Cleaner Engineering and Technology*, 4, 100215. https://doi.org/10.1016/j.clet.2021.100215
18. Nandipati, S., Srinivasa Rao, G. V. R., Manjunatha, M., Dora, N., and Bahij, S. (2023). Potential Use of Sustainable Industrial Waste Byproducts in Fired and Unfired Brick Production. *Advances in Civil Engineering*, 2023, Volume 2023, pp.ID 9989054. https://doi.org/10.1155/2023/9989054
19. Ogundiran, M. B., and Kumar, S. (2015). Synthesis and characterisation of geopolymer from Nigerian Clay. *Applied Clay Science*, 108, pp. 173–181. https://doi.org/10.1016/j.clay.2015.02.022
20. Phoo-ngernkham, T., Chindaprasirt, P., Sata, V., Hanjitsuwan, S., and Hatanaka, S. (2014). The effect of adding nano-SiO2 and nano-Al2O3 on properties of high calcium fly ash geopolymer cured at ambient temperature. *Materials and Design*, 55, pp.58–65. https://doi.org/10.1016/j.matdes.2013.09.049
21. Rai, S., Bahadure, S., Chaddha, M. J., and Agnihotri, A. (2020). Disposal Practices and Utilization of Red Mud (Bauxite Residue): A Review in Indian Context and Abroad. *Journal of Sustainable Metallurgy*, 6(1), pp. 1–8. https://doi.org/10.1007/s40831-019-00247-5
22. Rai, S., Wasewar, K. L., Lataye, D. H., Mishra, R. S., Puttewar, S. P., Chaddha, M. J., Mahindiran, P., and Mukhopadhyay, J. (2012). Neutralization of red mud with pickling waste liquor using Taguchi's design of experimental methodology. *Waste Management and Research*, 30(9), pp. 922–930. https://doi.org/10.1177/0734242X12448518

23. Rajesrajeswari, A., Dhinakaran, G., and Mohamed, E. (2014). Compressive strength of Silica Fume Based Geopolymer Concrete. *Asian Journal of Applied Science*, 7(4), pp. 240–247. https://doi.org/https://doi.org/10.3923/ajaps.2014.240.247
24. Reddy, P. S., Reddy, N. G., Serjun, V. Z., Mohanty, B., Das, S. K., Reddy, K. R., and Rao, B. H. (2021). Properties and Assessment of Applications of Red Mud (Bauxite Residue): Current Status and Research Needs. *Waste and Biomass Valorization*, 12(3), pp.1185–1217. https://doi.org/10.1007/s12649-020-01089-z
25. Saravanan, J., and Rao, P. V. (2023). Past investigations on development of sustainable bricks – A comprehensive review. *Sustainable Chemistry for the Environment*, *3*, 100030. https://doi.org/10.1016/j.scenv.2023.100030
26. Shill, S. K., Al-Deen, S., Ashraf, M., and Hutchison, W. (2020). Resistance of fly ash based geopolymer mortar to both chemicals and high thermal cycles simultaneously. *Construction and Building Materials*, 239. https://doi.org/10.1016/j.conbuildmat.2019.117886
27. Shivaprasad, K. N., and Das, B. B. (2018). Determination of optimized geopolymerization factors on the properties of pelletized fly ash aggregates. *Construction and Building Materials*, 163, pp.428–437. https://doi.org/10.1016/j.conbuildmat.2017.12.038
28. Siddique, R., and Chahal, N. (2011). Use of silicon and ferrosilicon industry by-products (silica fume) in cement paste and mortar. In *Resources, Conservation and Recycling* ,55(8), pp.739–744. https://doi.org/10.1016/j.resconrec.2011.03.004
29. Singh, S., Aswath, M. U., and Ranganath, R. V. (2020). Performance assessment of bricks and prisms: Red mud based geopolymer composite. *Journal of Building Engineering*, 32(3), pp.101462. https://doi.org/10.1016/j.jobe.2020.101462
30. Sontia Metekong, J. V., Kaze, C. R., Kamseu, E., Chinje, F. U., and Tatietse, T. T. (2024). Feasibility of production fired bricks based lateritic soil at very low temperature. *International Journal of Ceramic Engineering and Science*, 6(4), pp. e10225. https://doi.org/10.1002/ces2.10225
31. Sutar, H., Mishra, S. C., Sahoo, S. K., Chakraverty, A. P., and Maharana, H. S. (2014). Progress of Red Mud Utilization : An Overview. *American Chemical Science* , 4(3), pp.255–279. https://doi.org/https://doi.org/10.9734/ACSJ/2014/7258
32. Toniolo, N., Taveri, G., Hurle, K., Roether, J. A., Ercole, P., Dlouhý, I., and Boccaccini, A. R. (2017). Fly-ash-based geopolymers: How the addition of recycled glass or red mud waste influences the structural and mechanical properties. *Journal of Ceramic Science and Technology*, 8(3), pp. 411–419. https://doi.org/10.4416/JCST2017-00053
33. Turkey, F. A., Beddu, S. B., Ahmed, A. N., and Al-Hubboubi, S. K. (2022). Effect of high temperatures on the properties of lightweight geopolymer concrete based fly ash and glass powder mixtures. *Case Studies in Construction Materials*, 17, pp. e01489. https://doi.org/10.1016/j.cscm.2022.e01489

1